Hindawi
Journal of Chemistry
Volume 2019, Article ID 8464815, 8 pages
https://doi.org/10.1155/2019/8464815

Research Article

Adsorption of an Anionic Azo Dye Using *Moringa oleifera* Seed Protein-Montmorillonite Composite

Xiao Mi,[1,2,3] Zhenya Shang,[4] Chunbao Du,[5] Guoting Li,[1] Ting Su,[1] Xinying Chang,[1] Ruiming Li,[1] Zhihong Zheng,[6] and Jingxi Tie[1,2,3]

[1]*School of Environmental and Municipal Engineering, North China University of Water Resources and Electric Power, Zhengzhou 450011, China*
[2]*Henan Engineering Research Center of Water Pollution and Soil Damage Remediation, Zhengzhou 450011, China*
[3]*Henan Key Laboratory of Water Environment Simulation and Treatment, Zhengzhou 450011, China*
[4]*Henan Textile & Architecture Design Co. Ltd., Zhengzhou 450007, China*
[5]*College of Chemistry and Chemical Engineering, Xi'an Shiyou University, Xi'an 710065, China*
[6]*Henan Vocational College of Water Conservancy and Environment, Zhengzhou 450008, China*

Correspondence should be addressed to Zhihong Zheng; zzh_ncwu@163.com and Jingxi Tie; 15202843@qq.com

Received 18 December 2018; Revised 29 April 2019; Accepted 14 May 2019; Published 3 June 2019

Academic Editor: Hideto Miyabe

In this study, *Moringa oleifera* seed protein-montmorillonite (MOSP-MMT) composite was synthetized using the impregnation method. The MOSP-MMT adsorbent was characterized using scanning electron microscope, X-ray diffraction, infrared spectroscopy, surface area analysis, and thermogravimetric analysis. The removal of water-soluble reactive red 2 (RR-2) from artificial wastewater by the MOSP-MMT composite was carried out in a batch system. The results indicated that RR-2 adsorption increased with contact time, and the pseudo-second-order equation was best to describe the adoption process among the three models. The RR-2 adsorption decreased from 7.60 to 5.92 mg/g as pH increased from 3.2 to 9.1 and increased from 15.2 to 17.1 mg/g as NaCl concentration increased from 0 to 30 g/L. The Freundlich isotherm model provided the better fit of the experimental data than the Langmuir model. The result showed that the MOSP-MMT composite could be a potential adsorbent for the treatment of wastewater containing RR-2.

1. Introduction

Currently, most of the commercial dyes used in many industries including textile, paper, plastic, leather, and rubber have a synthetic origin. Dyes have physicochemical, thermal, and optical stability for the sake of their aromatic molecular structures, which in turn make them resistant to degrade with time, sunlight, and biological and chemical treatments [1, 2]. Furthermore, some dyes or their degradation intermediates are cancerogenic, teratogenic, and mutagenic [3, 4]. Hence, dyes must be removed before the dye-containing wastewater is discharged into water body. A lot of methods including chemical, physicochemical, and biological methods have been developed to treat dye-containing wastewater [5–8]. Among these techniques, adsorption is believed to be most promising because of its easy operation, low cost, and high performance without formation of harmful by-products. Seeking for the effective and efficient adsorbent is critical to ensure the success operation of adsorptive removal of dyes from their water solutions.

As a natural clay mineral, montmorillonite (MMT) has been used successfully for pollutants removal from contaminated water due to its advantages such as abundant reserve, low price, large specific surface area, good cation exchange capacity, excellent chemical and physical stability, versatility, and easy modification. [9, 10]. Unfortunately, the natural MMT has poor adsorption of anionic dyes due to the negative charge and hydrophilic characteristic of its surface [11]. Thus, many techniques have been used to modify MMT for improving its dye adsorption capacity [1, 12, 13], and organic modification of introducing active ligands to create

hybrid composites has been proved to be an important and successful strategy to increase the dye adsorption capacity of many materials [14, 15]. For instance, the adsorption capacity of direct blue 74 on poly(dopamine) grafted biosilica composite was 67.8 mg/g, and the capacity increased to 386.4 mg/g after tetraethylenepentamine ligands were loaded on the surface of the composite [16].

As a natural coagulant, *Moringa oleifera* seed protein (MOSP) has been proved to be very efficient for the removal of many negatively charged pollutants including anionic dyes since the protein is positively charged in the pH range below its isoelectric points between pH 10 and 11 [17–21].

In this study, the commercial MMT was modified with MOSP to create a new selective organ-montmorillonite for anionic dye adsorption. Hence, the main objective of this paper is to test the anionic dye adsorption of the *Moringa oleifera* seed protein-montmorillonite (MOSP-MMT) composite. Moreover, the parameters affecting the adsorption including contact time, pH, inorganic salt, and initial dye concentration were investigated.

2. Materials and Methods

2.1. Synthesis of MOSP-MMT Composite. The purified MMT was mixed with MOSP solution (8.14 g/L and pH = 6.8) at the approximate ratio of 1 : 3.2 (W : V) determined in our previous study, and the mixture was reacted in a shaker at 30°C for 24 h. The sediment collected after the centrifugation of the mixture at 8000 rpm for 10 min was washed with deionized water for 5 times and dried in a vacuum drying oven at 40°C in sequence. Finally, the dried composite was smashed and sieved for the experiment.

2.2. Preparation of Artificial Wastewater. A typical anionic dye, reactive red 2 (RR-2), was selected as the target pollutant. The RR-2 purchased from an online shop without further purification was dissolved into distilled water to synthesize the RR-2 solution. The pH value of the solution was adjusted using 0.1 M·NaOH and 0.1 M·HCl solutions and measured using a pH meter (pHS-3C, Leici Ltd., China). All the reagents used in this study were of analytical grade. The chemical structure of RR-2 is shown in Figure 1.

2.3. Adsorption Experiment. Static adsorption experiments were carried out to test the uptake of RR-2 by MMT-MOSP as functions of reaction time, pH, inorganic salt, and initial RR-2 concentration. The effect of reaction time on the adsorption of RR-2 was carried out at an initial RR-2 concentration of 51.9 and 100.3 mg/L at 30°C and pH 7. The influence of pH was studied at an initial RR-2 concentration of 52.6 mg/L in the pH range of 3.2–9.1 at 30°C with a reaction time of 10 h. The presence of salt on the uptake of RR-2 was studied at an initial RR-2 concentration of 42.5 mg/L at 30°C and pH 7 with reaction time of 10 h. The effect of initial RR-2 concentration on the removal effectiveness was conducted in the RR-2 concentration range of 47.0–380.9 mg/L at 20°C and 30°C, pH 7, and with a reaction time of 10 h. For every test, 0.05 g MOSP-MM and 10 mL

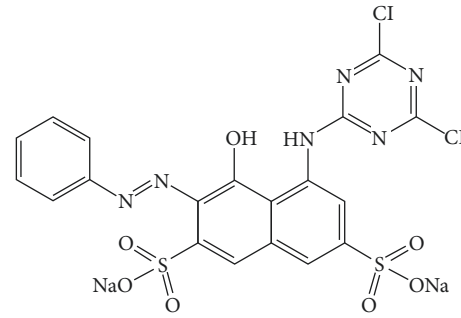

Figure 1: Chemical structure of RR-2 (chemical formula: $C_{19}H_{10}Cl_2N_6Na_2O_7S_2$ and molecular weight: 615.33).

RR-2 solution were used, and the shaking speed was 100 rpm. The pH values of the solutions were adjusted in the same way mentioned above. The mixture were centrifuged at 8000 rpm for 8 min to get the supernatants when the reaction was over, and the residual RR-2 concentrations in supernatants were determined using a UV-Vis spectrophotometer (UV-5100, Yuanxi Instruments, Shanghai, China) at its longest adsorption wavelength of $\lambda = 538$ nm [22].

The RR-2 uptake by MOSP-MMT was calculated using the following equation:

$$q = \frac{(C_0 - C_e)V}{m}, \quad (1)$$

where q is the RR-2 uptake by per unit MOSP-MMT (mg/g); C_0 and C_e (mg/L) are the initial and final RR-2 concentrations, respectively; V (L) is the RR-2 solution volume; and m is the amount of MOSP-MMT (g). The mean values of three independent experiments were used in the study.

2.4. Sample Characterization. The morphological information of the raw MMT and MOSP-MMT was characterized using SEM (JSM- 6460LV, Japan Electronic Co., Ltd.). MMT and MOSP-MMT were degassed at 90°C for 1 h, and then the temperature was increased to 300°C at the speed of 10°C per minute and kept at the temperature for 6 h before analysis. The surface areas were measured using the Brunauer–Emmett–Teller (BET) method at at −196°C (Autosorb-I, Quantachrome, USA). XRD patterns of the two samples were acquired with an X-ray diffractometer (Smartlab 3kw, Rigaku Ltd., Japan) over the scanning range of $2\theta = 2°$–$20°$ to study the changes in their structural properties. Bragg's law $2d \sin\theta = n\lambda$ was used to calculate the d_{001} of the two samples. FTIR spectra of MOSP, MMT, and MOSP-MMT were obtained using a FTIR spectrum (Nicolet 5700, Thermo Nicolet Ltd., USA) to observe the surface functional groups of the samples. The thermogravimetric analysis was carried out using the simultaneous thermal analyzer (STA409PC, NETZSCH group, Germany).

3. Results and Discussion

3.1. Sample Characterization. Figure 2(a) shows the SEM image of MMT and MOSP-MMT. There is no obvious difference between MMT and MOSP-MMT.

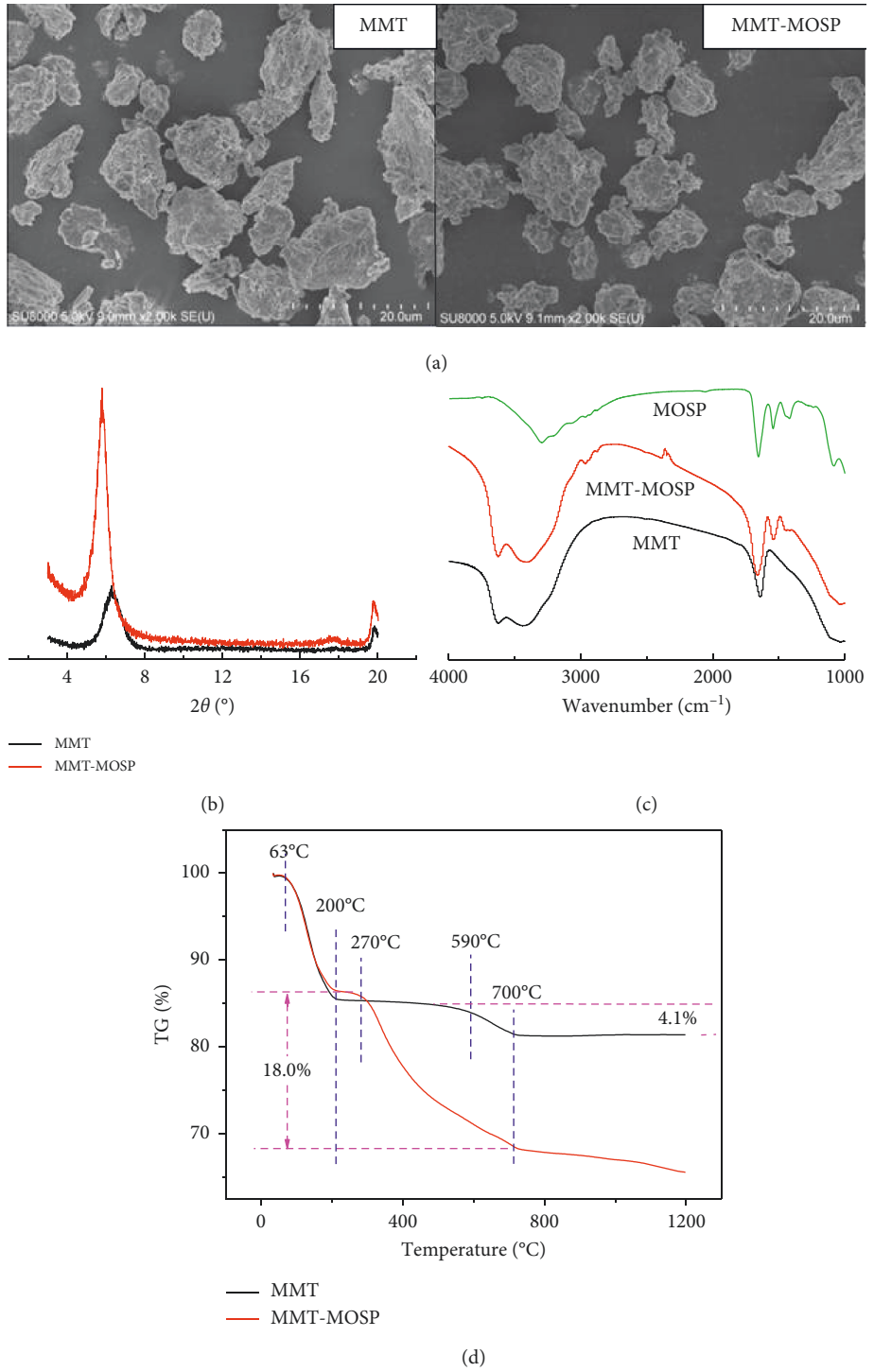

Figure 2: SEM of MMT and MOSP-MMT (a); XRD of MMT and MOSP-MMT (b); FTIR spectra of MMT, MOSP, and MOSP-MMT (c); TG of MMT and MOSP-MMT (d).

Figure 2(b) shows the XRD patterns of MMT and MOSP-MMT. The d_{001} reflection at 2θ for MMT and MOSP-MMT is 6.29 and 5.82°, and their corresponding interlayer spacings are 14.2 and 15.2 Å, respectively. Considering the large spatial structure of MOSP, it was impossible for the MOSP to enter the interlayer of MMT, and the increase of the interlayer was probably caused by the existence of the small molecule such as H_2O with the bond length of about 1.0 Å. Thus, it could be confirmed that MOSP was only adsorbed on the surface of MMT.

Figure 2(c) shows the FTIR results of MOSP, MMT, and MOSP-MMT. The characteristic bands at 1659, 1543, and 1237 cm^{-1} in the MOSP spectrum were assigned to C=O stretching (amide I), CN stretching, and NH bonding (amide

II) and CN stretching (amide III), respectively. A new band at 1540 cm^{-1} appeared in the MOSP-MMT, indicating the reaction of MOSP with MMT.

Figure 2(d) shows the thermogravimetric results of MMT and MOSP-MMT. It can be seen that both MMT and MOSP-MMT lost absorbed water on its surface and interlayer water below 200°C. MMT lost residual interlayer water and hydroxyl in the temperature range of 590–700°C. MOSP in MOSP-MMT decomposed and carbonized in the temperature range of 270–700°C. MOSP-MMT was thermostable below 63°C. The mass proportion of MOSP in MOSP-MMT was about 13.9%.

Table 1 summarizes the BET parameters of MMT and MOSP-MMT. MMT showed the specific surface area of 21.91 m^2/g and total pore volume of 0.090 cm^3/g with the average pore size of 16.38 nm. After the modification by MOSP, the specific surface area and total pore volume of MOSP-MMT decreased to 4.90 m^2/g and 0.025 cm^3/g, respectively, with the average pore size of 20.94 nm, which might result from the fact that the pores in MMT were occupied by MOSP.

3.2. Effect of Reaction Time and Kinetics Study. Figure 3 shows the effect of reaction time on RR-2 uptake at two initial RR-2 concentrations. It can be seen that the adsorption of RR-2 on MOSP-MMT can be divided into a fast and a slow stage for both of the two concentrations. The fast stage lasted from the beginning to the 15th min when MOSP-MMT offered more free active sites in this stage, indicating that chemical adsorption might be the main mechanism for RR-2 uptake in this stage. There were less and less active sites left for the adsorption in the following slow stage to slow down the adsorption. Additionally, the repulsion between the absorbed and the free dye molecules in solution further weakened the reaction.

To further understand the adsorption, three classic kinetic equations including pseudo-first-order, pseudo-second-order, and Elovich equations are used to describe the adsorption.

The linearized form of the pseudo-first-order equation is shown as follows:

$$\log(q_e - q_t) = \log q_e - \frac{k_1}{2.303}t, \tag{2}$$

where q_t and q_e (mg/g) are the RR-2 uptake at time t and at equilibrium, respectively; k_1 (min^{-1}) is the equilibrium rate constant; and k_1 and predicted q_e could be obtained from the slope and intercept of the plot of log $(q_e - q_t)$ vs t.

The linearized form of the pseudo-second-order equation is shown as follows:

$$\frac{t}{q_t} = \frac{t}{q_e} + \frac{1}{k_2 q_e^2}, \tag{3}$$

where k_2 (g/(mg·min)) is the equilibrium rate constant and k_2 and q_e could be determined from the slope and intercept of the plot of t/q_t vs t.

Table 1: BET parameters of MMT and MOSP-MMT.

Samples	Specific surface area (m^2/g)	Total pore volume (cm^3/g)	Average pore size (nm)
MMT	21.91	0.090	16.38
MOSP-MMT	4.90	0.025	20.94

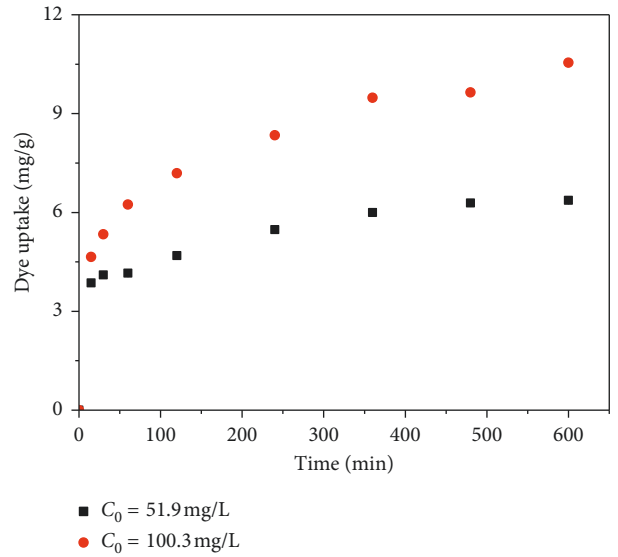

Figure 3: Effect of reaction time on RR-2 uptake (T = 30°C and pH = 7.0).

The linearized form of the Elovich equation is shown as follows:

$$q_t = \frac{1}{\beta}\ln(\alpha\beta) + \frac{1}{\beta}\ln t, \tag{4}$$

where α (mg/(g min)) and β (g/mg) are the initial adsorption rate and the constant associated with the fraction of surface coverage and activation energy for chemisorption, respectively. The two parameters could be determined from the intercept and slope of the plot of q_t vs. lnt.

The kinetics parameters obtained from the three linearized plots are shown in Table 2. The correlation coefficients of the pseudo-second-order kinetics are highest among the three models. The calculating values of $q_{e,cal}$ got from the equations are in good accordance with those values of $q_{e,exp}$ obtained from the experiments, indicating that the adsorption followed the pseudo-second-order kinetics. Thus, chemical adsorption or chemisorption might be the rate-determining step for the adsorption of RR-2 on MOSP-MMT, and the valency force between the RR-2 molecular and MOSP-MMT might be involved in the adsorption as well.

3.3. Effect of pH. Solution pH can impact both the surface charges of adsorbent and the existing forms of adsorbate [23, 24], which in turn affects the adsorption. Figure 4 shows the effect of pH on RR-2 uptake. RR-2 uptake decreased from 7.6 to 6.5 mg/g as the pH increased from 3.2 to 4.1, and the RR-2 uptake decreased to 5.9 gradually as the pH rose to

Table 2: Parameters of the three kinetic equations for RR-2 adsorption on MOSP-MMT.

Models	Parameters	Values	
		$C_0 = 51.9$ mg/L	$C_0 = 100.3$ mg/L
Pseudo-first-order equation	$q_{e,exp}$	6.3	10.5
	$q_{e,cal}$	6.51	3.12
	k_1	0.0039	0.0053
	R^2	0.964	0.9
Pseudo-second-order equation	$q_{e,cal}$	6.60	10.81
	k_2	0.0050	0.0021
	R^2	0.9959	0.9918
Elovich equation	α	5.71	1.58
	β	1.35	0.63
	R^2	0.9357	0.9796

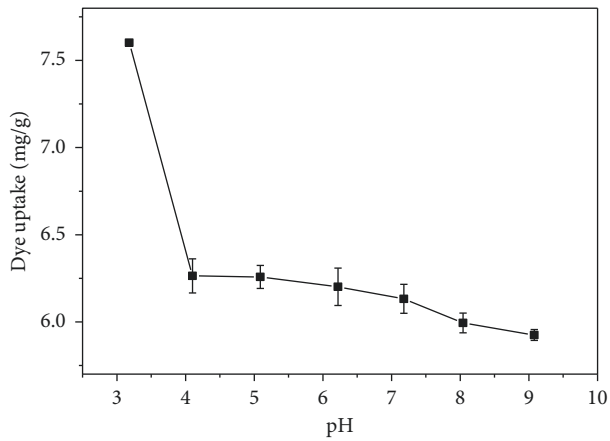

Figure 4: Effect of pH on RR-2 uptake (C_0: 52.6 mg/L, T: 30°C, and time: 10 h).

9.1. Overall, rising pH weakened the RR-2 uptake. MMT could hardly adsorb RR-2 (data not shown) due to its hydrophilicity and net negative charge. However, the MOSP-MMT could adsorb RR-2 since the positively charged amino groups of MOSP in the MOSP-MMT could react with anionic groups of the RR-2 in the pH range of 3–9 set for the experiment, which improved the RR-2 adsorption. The probable mechanism for RR-2 adsorption on MOSP-MMT could be described by the following equations. P is used to represent the coagulating protein since its structure is still unknown so far:

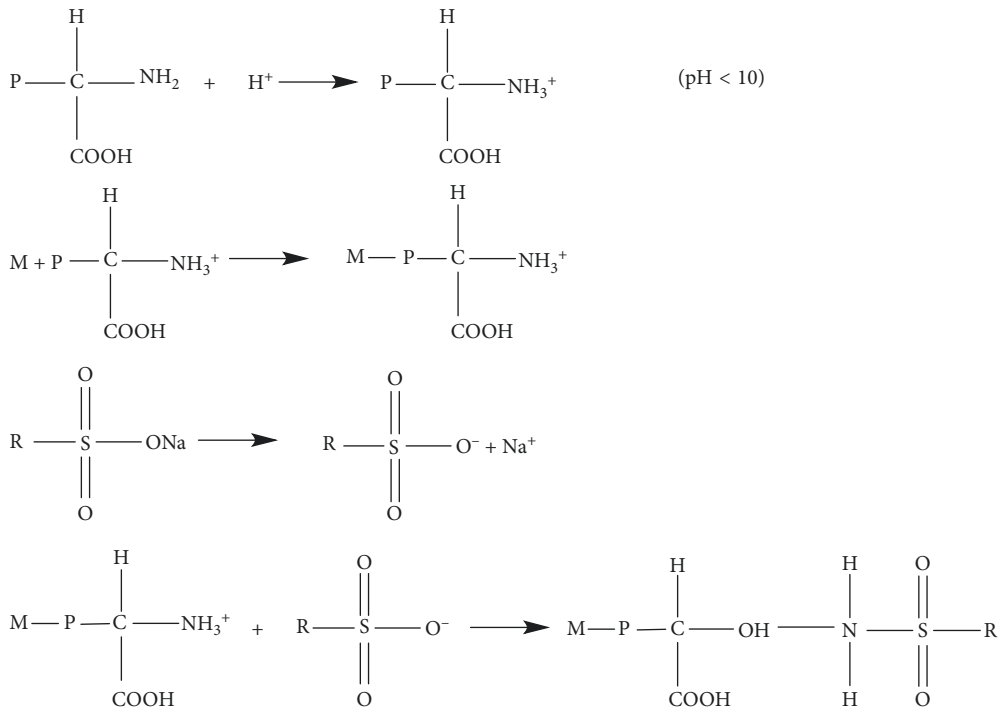

(5)

where *P*, *M*, and *R* denote MOSP, MMT, and RR-2, respectively.

The weakened adsorption with the increasing pH could be explained by the fact that the negative charge of RR-2 and positive charge on MOSP-MMT surface decreased with the rising pH. Additionally, the competition between RR-2 molecules and increasing OH^- groups for the active sites weakened the RR-2 uptake as well.

3.4. Effect of Inorganic Salt. NaCl is an inorganic salt used widely to prompt dyeing efficiency because it can drive the dye molecules out of solution onto fibers [25]. Thus, there are a large amount of NaCl in dye-containing wastewater. Hence, the effect of NaCl on RR-2 removal was investigated. Figure 5 shows that RR-2 uptake increased from 15.2 to 17.1 mg g^{-1} as NaCl increased from 0 to 30 g/L, indicating that NaCl can improve the removal of RR-2. In

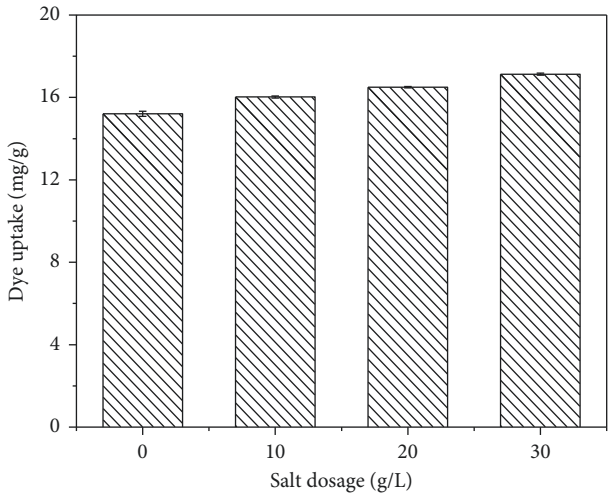

Figure 5: Effect of inorganic salt (C_0: 142.5 mg/L, T: 30°C, reaction time: 10 h, and pH: 7).

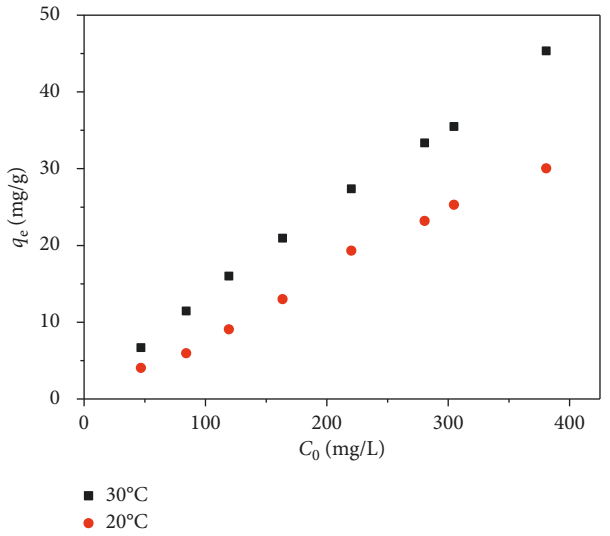

Figure 6: Effect of initial RR-2 concentration (reaction time: 10 h and pH: 7).

our previous study, we found NaCl could increase the adsorption of reactive green on polyaniline/bentonite as well [25]. Ip et al. reported that the adsorption capacities of reactive dyes on four adsorbents increased with rising NaCl concentration as well [26]. The rise of the dye uptake caused by NaCl addition was attributed to the aggregation of reactive dye molecules resulted from the increased intermolecular forces, including van der Waals forces, ion-dipole forces, and dipole-dipole forces [27]. Additionally, the salts interacted with the adsorbate and screened the repulsive force between the dye molecules and the carbon surface between the adsorbed species [26], which could be another explanation for the increase of RR-2 removal.

3.5. Effect of Initial RR-2 Concentration. Figure 6 shows the effect of initial RR-2 concentration on its adsorption on MOSP-MMT. Effect of initial RR-2 concentration on its adsorption was carried out ranging from 47.0 to 380.9 mg/L. Figure 6 clearly reveals that the extent of adsorption of RR-2 increased linearly with the rising RR-2 concentration. Meanwhile, at every RR-2 concentration, RR-2 adsorption at 30°C was better than that at 20°C.

The adsorption isotherm gives an idea of how the adsorbate molecules distribute between the liquid-solid interface at equilibrium [28, 29], which helps us to further understand the nature of adsorption. Thus, the Langmuir and Freundlich models are adopted to analyze the adsorption data at equilibrium, as shown in Figure 7.

The linearized form of the Langmuir equation is shown as follows:

$$\frac{c_e}{q_e} = \frac{1}{q_m b} + \frac{c_e}{q_m}, \quad (6)$$

where c_e (mg/L) and q_e (mg/g) are the concentration and adsorption capacity at equilibrium, respectively, and b (L/mg) and q_m (mg/g) are the Langmuir constant related to binding energy and the maximum adsorption capacity, respectively,

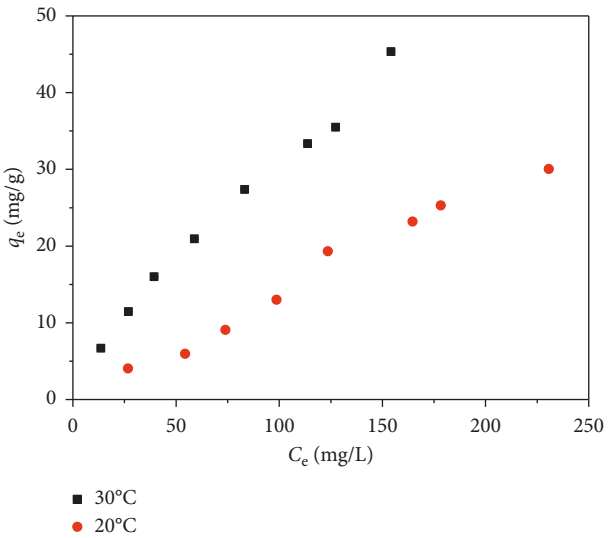

Figure 7: Adsorption isotherm of RR-2 on MOSP-MMT at two temperatures (initial RR-2 concentration: 47.0 mg/L–380.9 mg/L, reaction time: 10 h, and pH: 7).

which could be obtained from the slope and intercept of the plots of $1/c_e$ versus c_e/q_e, respectively.

The linearized form of the Freundlich equation is shown as follows:

$$\log q_e = \log k_f + \frac{1}{n} \log C_e, \quad (7)$$

where q_e (mg/g) and c_e (mg/L) have same meaning as that mentioned above and k_f and n are the Freundlich constants related to adsorption capacity and adsorption intensity, respectively, which could be obtained from the slope and intercept of the plots of $\ln c_e$ versus $\ln q_e$, respectively.

Parameters of Langmuir and Freundlich isotherms are shown in Table 3. It can be seen that the R^2 values of

Table 3: Parameters of Langmuir and Freundlich isotherms.

	20°C	30°C
Langmuir		
q_m	—	93.45
b	−2991.27	0.0052
R^2	0.0408	0.9138
Freundlich		
n	0.9834	0.8270
k_f	0.1246	0.0666
R^2	0.9754	0.9972

isotherm at both of the two temperatures are better than those of Langmuir isotherm, indicating that the Freundlich equation is more suitable to describe the adsorption of RR-2 on MOSP-MMT, which was a multilayer adsorption of RR-2 on the heterogeneous surface MOSP-MMT [30].

4. Conclusion

In the present study, MOSP-MMT composite was synthesized and characterized, and the adsorption properties of the composite were investigated with a typical reactive dye, namely, RR-2. The adsorption process was found to be dependent on contact time, pH, inorganic salt, and initial dye concentration and the adsorption process followed the pseudo-second-order kinetics. The data obtained from adsorption isotherms at two temperatures fitted to the Freundlich model better than the Langmuir model. The composite has considerable potential for the removal of RR-2 from water solution.

Data Availability

The data used to support the findings of this study are available from the corresponding author upon request.

Conflicts of Interest

The authors declare that they have no conflicts of interest.

Acknowledgments

This work was supported by the Science and Technology Major Project of Henan Province (Grant number: 161100310700).

References

[1] P. Monvisade and P. Siriphannon, "Chitosan intercalated montmorillonite: preparation, characterization and cationic dye adsorption," *Applied Clay Science*, vol. 42, no. 3-4, pp. 427–431, 2009.

[2] F. A. R. Uddin, K. S. Sousa, G. R. S. Cavalcanti et al., "Green biosorbents based on chitosan-montmorillonite beads for anionic dye removal," *Journal of Environmental Chemical Engineering*, vol. 5, no. 4, pp. 3309–3318, 2017.

[3] J. L. Gong, B. Wang, G. M. Zeng et al., "Removal of cationic dyes from aqueous solution using magnetic multi-wall carbon nanotube nanocomposite as adsorbent," *Journal of Hazardous Materials*, vol. 164, no. 2-3, pp. 1517–1522, 2009.

[4] L. Tang, Y. Cai, G. Yang et al., "Cobalt nanoparticles-embedded magnetic ordered mesoporous carbon for highly effective adsorption of rhodamine B," *Applied Surface Science*, vol. 314, pp. 746–753, 2014.

[5] C. S. Ayyappan, V. M. Bhalambaal, and S. Kumar, "Effect of biochar on bio-electrochemical dye degradation and energy production," *Bioresource Technology*, vol. 251, pp. 165–170, 2018.

[6] R. Li, B. Gao, K. Guo, Q. Yue, H. Zheng, and Y. Wang, "Effects of papermaking sludge-based polymer on coagulation behavior in the disperse and reactive dyes wastewater treatment," *Bioresource Technology*, vol. 240, pp. 59–67, 2017.

[7] C. Liu, A. M. Omer, and X.-K. Ouyang, "Adsorptive removal of cationic methylene blue dye using carboxymethyl cellulose/k-carrageenan/activated montmorillonite composite beads: isotherm and kinetic studies," *International Journal of Biological Macromolecules*, vol. 106, pp. 823–833, 2018.

[8] M. A. Talha, M. Goswami, B. S. Giri, A. Sharma, B. N. Rai, and R. S. Singh, "Bioremediation of Congo red dye in immobilized batch and continuous packed bed bioreactor by Brevibacillus parabrevis using coconut shell biochar," *Bioresource Technology*, vol. 252, pp. 37–43, 2018.

[9] B. Ma, S. Oh, W. S. Shin, and S. J. Choi, "Removal of Co^{2+}, Sr^{2+} and Cs^{+} from aqueous solution by phosphate-modified montmorillonite (PMM)," *Desalination*, vol. 276, no. 1–3, pp. 336–346, 2011.

[10] R. Zhu, Q. Chen, Q. Zhou, Y. Xi, J. Zhu, and H. He, "Adsorbents based on montmorillonite for contaminant removal from water: a review," *Applied Clay Science*, vol. 123, pp. 239–258, 2016.

[11] Y. Li, X. Hu, X. Liu et al., "Adsorption behavior of phenol by reversible surfactant-modified montmorillonite: mechanism, thermodynamics, and regeneration," *Chemical Engineering Journal*, vol. 334, pp. 1214–1221, 2018.

[12] H.-P. Ren, S.-P. Tian, M. Zhu et al., "Modification of montmorillonite by gemini surfactants with different chain lengths and its adsorption behavior for methyl orange," *Applied Clay Science*, vol. 151, pp. 29–36, 2018.

[13] M. M. F. Silva, M. M. Oliveira, M. C. Avelino, M. G. Fonseca, R. K. S. Almeida, and E. C. S. Filho, "Adsorption of an industrial anionic dye by modified-KSF-montmorillonite: evaluation of the kinetic, thermodynamic and equilibrium data," *Chemical Engineering Journal*, vol. 203, pp. 259–268, 2012.

[14] T. A. Arica, E. Ayas, and M. Y. Arica, "Magnetic MCM-41 silica particles grafted with poly (glycidylmethacrylate) brush: modification and application for removal of direct dyes," *Microporous and Mesoporous Materials*, vol. 243, pp. 164–175, 2017.

[15] G. Bayramoglu and M. Y. Arica, "Removal of reactive dyes from wastewater by acrylate polymer beads bearing amino groups: isotherm and kinetic studies," *Coloration Technology*, vol. 129, no. 2, pp. 114–124, 2013.

[16] T. A. Arica, M. Kuman, O. Gercel, and E. Ayas, "Poly (dopamine) grafted bio-silica composite with tetraethylenepentamine ligands for enhanced adsorption of pollutants," *Chemical Engineering Research and Design*, vol. 141, pp. 317–327, 2019.

[17] A. Ndabigengesere, K. S. Narasiah, and B. G. Talbot, "Active agents and mechanism of coagulation of turbid waters using *Moringa oleifera*," *Water Research*, vol. 29, no. 2, pp. 703–710, 1995.

[18] M. Pritchard, T. Craven, T. Mkandawir, A. S. Edmondson, and J. G. O'Neill, "A comparison between *Moringa oleifera* and chemical coagulants in the purification of drinking water-an alternative sustainablesolution for developing countries,"

Physics and Chemistry of the Earth, vol. 35, no. 13–15, pp. 798–805, 2010.

[19] J. Tie, M. Jiang, H. Li, S. Zhang, and X. Zhang, "A comparison between *Moringa oleifera* seed presscake extract and polyaluminum chloride in the removal of direct black 19 from synthetic wastewater," *Industrial Crops and Products*, vol. 74, pp. 530–534, 2015.

[20] J. Tie, P. Li, Z. Xu, Y. Zhou, C. Li, and X. Zhang, "Removal of Congo red from aqueous solution using *Moringa oleifera* seed cake as natural coagulant," *Desalination and Water Treatment*, vol. 54, no. 10, pp. 2817–2824, 2015.

[21] J. Tie, Z. Zheng, X. Zheng, and Y. Hao, "Comparison of the performance of *Moringa oleifera* seed protein and polyaluminum chloride in removal of humic acid from water," *Desalination and Water Treatment*, vol. 90, pp. 214–219, 2017.

[22] C.-C. Lin, Y.-S. Lin, and J.-M. Ho, "Adsorption of reactive red 2 from aqueous solutions using Fe_3O_4 nanoparticles prepared by co-precipitation in a rotating packed bed," *Journal of Alloys and Compounds*, vol. 666, pp. 153–158, 2016.

[23] X. Wu, D. Wu, and R. Fu, "Studies on the adsorption of reactive brilliant red X-3B dye on organic and carbon aerogels," *Journal of Hazardous Materials*, vol. 147, no. 3, pp. 1028–1036, 2007.

[24] C. Wang, S. Yang, H. Chen, H. He, and C. Sun, "Adsorption behavior and mechanism of reactive brilliant red X-3B in aqueous solution over three kinds of hydrotalcite-like LDHs," *Applied Surface Science*, vol. 301, pp. 329–337, 2014.

[25] J. Tie, D. Chen, M. Zhao, X. Wang, S. Zhou, and L. Peng, "Adsorption of reactive green 19 from water using polyaniline/bentonite," *Journal of Water Reuse and Desalination*, vol. 6, no. 4, pp. 515–523, 2016.

[26] A. W. M. Ip, J. P. Barford, and G. McKay, "Reactive black dye adsorption/desorption onto different adsorbents: effect of salt, surface chemistry, pore size and surface area," *Journal of Colloid and Interface Science*, vol. 337, no. 1, pp. 32–38, 2009.

[27] G. Alberghina, R. Bianchini, M. Fichera, and S. Fisichella, "Dimerization of cibacron blue F3GA and other dyes: influence of salts and temperature," *Dyes and Pigments*, vol. 46, no. 3, pp. 129–137, 2000.

[28] B. H. Hameed, I. A. W. Tan, and A. L. Ahmad, "Adsorption isotherm, kinetic modeling and mechanism of 2,4,6-trichlorophenol on coconut husk-based activated carbon," *Chemical Engineering Journal*, vol. 144, no. 2, pp. 235–244, 2008.

[29] Z. G. Peng, K. Hidajat, and M. S. Uddin, "Selective and sequential adsorption of bovine serum albumin and lysozyme from a binary mixture on nanosized magnetic particles," *Journal of Colloid and Interface Science*, vol. 281, no. 1, pp. 11–17, 2005.

[30] D. Vu, Z. Li, H. Zhang et al., "Adsorption of Cu(II) from aqueous solution by anatase mesoporous TiO_2 nanofibers prepared via electrospinning," *Journal of Colloid and Interface Science*, vol. 367, no. 1, pp. 429–435, 2012.